DOI: 10.1002/ejic.200700628

Synthesis, Structure and a DFT/TDDFT Study of a Diimido-Bridged Asymmetric Dimolybdenum Complex

Kuntal Pal[a] and Sabyasachi Sarkar*[a]

In memory of Professor Frank Albert Cotton

Keywords: Mixed-valence compounds / Molybdenum / Cyclic voltammetry / Electronic structure / Density functional calculations

The homobimetallic complex $(Bu_4N)_2$[MoO(mnt)Mo{*o*-aminobenzothiolato(3–)-*N*,*S*}$_2$(mnt)] (**2**; mnt = 1,2-dicyanoethylenedithiolate) has been synthesized as a dark green solid by treating $(Bu_4N)_2[Mo_2O_4(mnt)_2]$ (**1**) with *o*-aminothiophenol in CH_3CN. An X-ray crystal structure analysis of **2** reveals that it possesses an asymmetric structure where one Mo has a distorted octahedral geometry and the other a square-pyramidal geometry. The basal plane of the two Mo centers makes an angle of 26.41°, which is nearly one quarter of 90°. The shape of the ν(Mo=O) band in the IR spectrum of **2** suggests that these Mo atoms may have different oxidation states. The different reactivity of **1** with *o*-aminothiophenol and 2-aminoethanethiol was followed by EPR spectroscopy, and analysis of the different end-products from these reactions supports the proposal that **2** is a mixed-valence compound containing Mo^{VI} and Mo^{IV} centers. The electronic structures of **1** and **2** have been calculated at the DFT level of theory to analyse the effect of a deviation of the basal plane on the metal–metal bond in **2**. The cyclic voltammetric responses of **1** and **2** have been measured to correlate the data with the computational results. TDDFT calculations have been performed on **1** and **2** in the gas phase and also in a solvent medium to assign the transitions corresponding to the peaks found in the respective experimental electronic absorption spectra of these complexes.

Introduction

Terminal oxido- or sulfido-coordinated higher-valent Mo complexes with dithiolene as co-ligand are good models for molybdenum-based enzymes.[1,2] Hexacoordinate Mo^{VI} complexes[3] generally adopt a distorted octahedral geometry with *cis* dioxido or oxido-sulfido groups, whereas related Mo^{IV} complexes generally adopt a square-pyramidal geometry[4] with a terminal Mo=O group or trigonal biprismatic geometry with a terminal Mo–SR (thiolato) moiety.[5] Molybdenum(V) complexes[6] are generally stabilized by di-μ_2-oxido or mono-μ_2-oxido bridging groups and have the general formula $\{M_2X_2Y_2\}^{2+}$, where X (terminal group) and Y (bridging group) are a combination of O and S atoms. The stability of di-μ_2-oxido-bridged dimeric Mo^V complexes arises from a strong Mo(d_{xy})–Mo(d_{xy}) σ bond[7,8] supplemented by pπ bonding between the bridging ligand atoms and the two Mo atoms, which remain almost in the same plane. Imidomolybdenum complexes, which are isoelectronic to oxido complexes, are also known,[9,10] and two Lewis structures have been proposed for the Mo–N binding mode of the imido group to Mo (Scheme 1).[11] In the first, the nitrogen atom acts as a four-π-electron donor and Mo–N–R angle is close to 180°, whereas in the second the nitrogen atom acts as a two-electron donor and the Mo–N–R linkage is bent. The majority of monomeric Mo-imido complexes have a linear imido linkage and most imido-bridged Mo complexes have a bent imido linkage.

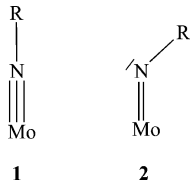

1 **2**

Scheme 1. Two possible binding modes of the imido group at an Mo center.

Dialkyldithiocarbamato (dtc)-coordinated dimeric Mo^V complexes with terminal and/or bridging imido linkages have been synthesized from the corresponding oxido and/or sulfido complexes[9] by substitution reactions. Most Mo^{VI}-imido complexes[10] have a linear Mo–N–R linkage. The re-

[a] Department of Chemistry, Indian Institute of Technology Kanpur,
Kanpur 208016, India
Fax: +91-512-2597265
E-mail: abya@iitk.ac.in

Supporting information for this article is available on the WWW under http://www.eurjic.org or from the author.

action of a dtc-coordinated oxido-Mo^{VI} complex with 2-aminothiophenol has been reported to produce the intermediate imido complex $[Mo^{VI}(dtc)_2(NC_6H_4S)(OCH_3)]$,[11] which reacts further to give $[Mo^{V}O(dtc)(\mu_2\text{-}NC_6H_4S)_2\text{-}Mo^{V}(dtc)]$ on heating in the solid state under vacuum. The chemistry of oxidomolybdenum complexes varies with the co-ligand, which ranges from dtc to dithiolene-type ligands such as 1,2-dicyanoethenedithiolate (mnt).[12] Although both these co-ligands are sulfur donor bidentate ligands they differ in the bite angle on coordination to the Mo center. In this article we report the reaction of 2-aminothiophenol with a symmetrical di-μ_2-oxido Mo^{V} dithiolene complex to form an asymmetric dimeric dimolybdenum mnt-coordinated complex. The di-μ_2-oxido groups are replaced by imido coordination arising from coordination of the deprotonated 2-aminothiophenol to asymmetric oxidomolybdenum and desoxomolybdenum centers. The reaction is followed by EPR spectroscopy to understand its course, and DFT and TDDFT calculations of the synthesized complex have been carried out to correlate its spectral properties with electronic structure.

Results and Discussion

Synthesis and IR Studies

The dithiolene-coordinated dimeric Mo^{V} complex $[Bu_4N]_2[Mo_2O_4(mnt)_2]$ (**1**) has been reported recently.[6a] One of the di-μ_2-oxido groups in **1** is readily protonated in the presence of a weak acid and the conjugate base of the acid then coordinates to the metal center to give linear mono μ_2-oxido-bridged dimeric Mo^{V} complexes with the general formula $[Mo_2O_3(mnt)_2(X)_2]^-$ [X = SPh (**1a**), Cl (**1b**), and Br (**1c**)].[6a] It has been shown that **1a**–**c**, which possess an $\{Mo_2O_3\}^{2+}$ core, hydrolyze back to **1** in the presence of traces of moisture via an EPR-active monomeric $[MoO(mnt)(X)(OH)]^-$ species. This EPR-active intermediate is readily dimerized to a stable di-μ_2-oxido-bridged form due to the presence of two monodentate ligands in adjacent equatorial positions. Our goal was to synthesize a monomeric Mo^{V} species with three S donor atoms (two from a dithiolene ligand and one from an SR group) to mimic the half-reduced state of sulfite oxidase.[13] The vacant fourth site in the equatorial plane of the expected square-based pyramidal Mo complex could be filled by an N-donor therefore we decided to use 2-aminothiophenol and 2-aminoethanethiol, both of which provide one S and one N atom. Both these ligands are in a zwitterionic form in solution, like an amino acid, although 2-aminoethanethiol, unlike 2-aminothiophenol, lacks π delocalization. Treatment of **1**, **1a**, **1b**, or **1c** with 2-aminothiophenol in dichloromethane causes the color of the solution to change to light green, which suggests the formation of a new species, although addition of petroleum ether allowed only **1** to be isolated. The light-green species is EPR-active and the isolation of only **1** from such a reaction mixture clearly suggests that the 2-aminothiophenolato-coordinated Mo^{V} monomer (EPR active) is in equilibrium with **1** in solution and that addition of the second solvent shifts the equilibrium towards **1**. The use of a more polar solvent such as acetonitrile led to a similar reactivity, whereas employing more drastic reaction conditions changed the course of the reaction. Thus, refluxing **1** with 2-aminothiophenol in acetonitrile yielded **2**. Unlike dtc-coordinated Mo complexes, however, **1** does not react with aniline or substituted anilines.

Addition of a solution of 2-aminoethanethiol in methanol to an acetonitrile solution of **1** caused a color change of the reaction mixture from yellow to dark-orange and finally to green, followed by immediate precipitation of yellow $[Mo^{VI}O_2(SCH_2CH_2NH_2)]$[14] in 48% yield. Further workup yielded 46% of $[(Bu_4N)_2][Mo^{IV}O(mnt)_2]$ from the mother liquor (Scheme 2). Reaction of $[Mo^{VI}O_2(mnt)_2]^{2-}$ with 2-aminothiphenol or 2-aminoethanethiol yielded $[Mo^{IV}O(mnt)_2]^{2-}$ quantitatively, with no formation of any imido-coordinated complex.[15] Similar reactions of these aminothiols with dtc-coordinated Mo^{VI} complexes have shown a different chemistry.[10]

On the basis of the total charge and the diamagnetic nature of **2**, the possible formal oxidation states of the two Mo(1)/Mo(2) centers are either +5/+5 or +6/+4. This question can be resolved by considering the Mo=O stretching vibration of this unsymmetrical complex as the ν(Mo=O) vibration in molybdenum complexes is sensitive to the formal oxidation state of Mo. Thus, this vibration in pentacoordinate bis-dithiolene Mo^{IV} complexes[16] generally appears below 940 cm^{-1}, whereas in related Mo^{V} species it

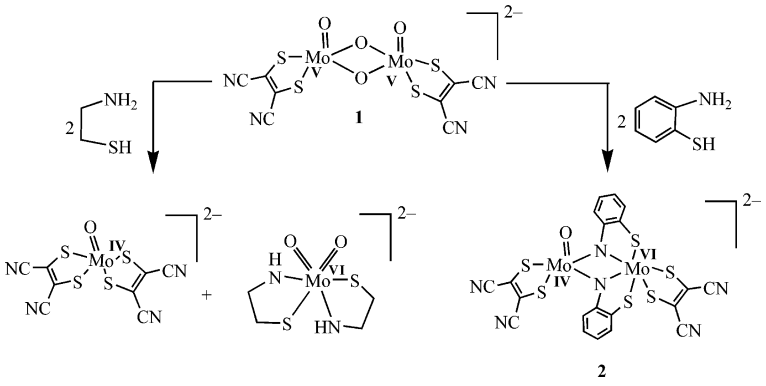

Scheme 2. Reaction of $(Bu_4N)_2[Mo^{V}_2O_4(mnt)_2]$ (**1**) with 2-aminothiophenol and 2-aminoethanethiol.

Table 1. Values of ν(Mo=O) [cm^{-1}] for selected Mo complexes.

Complexes	ν(Mo=O_t)[a]	Ref.
$[Mo_2O(mnt)_2\{o\text{-aminobenzothiolato}(3-)\text{-}N,S\}_2]^{2-}$	937	this work
$[Mo^{IV}O(mnt)_2]^{2-}$	932	[3c]
$[Mo^{IV}O(mnt)(Bu_2bpy)]$	939	[4d]
$[Mo^{V}{}_2O_4(mnt)_2]^{2-}$	977	this work
$[Mo^{V}{}_2O_2(mnt)_2(\mu\text{-SPh})_2(\mu\text{-OR})]^{-1}$ (R = Me, Et, *i*Pr)	951, 958, 961	[6a]
$[Mo^{V}{}_2O_2(mnt)_2(\mu\text{-O})(\mu\text{-SPh})(\mu\text{-Br})]^{-2}$	960	[6a]
$[Mo^{V}{}_2O_2(mnt)_2(\mu\text{-O})(\mu\text{-SPh})(\mu\text{-CH}_3SO_3)]^{-2}$	957	[6a]
$[Mo^{V}{}_2O_2(mnt)_2(\mu\text{-O})(\mu\text{-SEt})(\mu\text{-CH}_3SO_3)]^{-2}$	952	[6a]

[a] t = terminal.

appears above 950 cm^{-1} (Table 1). The appearance of ν(Mo=O) at 937 cm^{-1} in **2** therefore indicates that the Mo(2) center is formally in the Mo^{IV} state, which fixes the oxidation state of Mo(1) as +6.

EPR Studies

The reaction leading to **2** involves the initial formation of an EPR-active Mo^{V} species. This intermediate could not be identified in the case of 2-aminoethanthiol as rapid precipitation of yellow $[Mo^{VI}O_2(SCH_2CH_2NH_2)]$[14] from the reaction mixture took place with the formation of an equivalent amount of $[(Bu_4N)_2][Mo^{IV}O(mnt)_2]$.[14] Such a behavior can be explained by a disproportionation reaction where removal of the oxidized part of the product as a solid drives the reaction quickly to completion. In contrast, a similar reaction with 2-aminothiophenol led to the formation of an EPR-active Mo^{V} signal (Figure 1) which was stable for hours, thereby indicating the inability of the complex formed to undergo a disproportionation reaction.

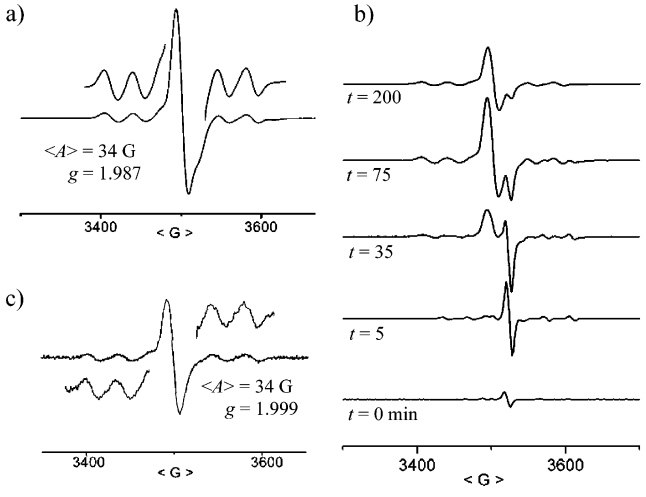

Figure 1. EPR spectra of the reaction of $(Bu_4N)_2[Mo^{V}{}_2O_4(mnt)_2]$ (**1**) with 2-aminothiophenol in acetonitrile at room temperature: a) at the initial stage (5 min), $<A>$ = 34 G, g = 1.987; b) EPR signal at different time intervals showing the appearance of another EPR active species ($<A>$ = 34 G, g = 1.999); c) after 24 h.

Attempts to isolate this species were unsuccessful and only the starting complex **1** was obtained. We were able to identify the formation of an intermediate Mo^{V} species ($<g>$ = 1.987; Figure 1, a) in the initial stages of the reaction which was stable for a long time and only disappeared on heating the solution. This EPR signal is associated with another EPR Mo^{V} signal ($<g>$ = 1.999; Figure 1), although this second signal remains even after the disappearance of the main EPR signal (Figure 1, c). The broad nature of the EPR signal (13 G) prevented us from identifying any superhyperfine interaction arising from nearby protons. Changing the reaction medium to a less polar solvent like dichloromethane did not help to reduce the line width. In the frozen state (liquid nitrogen), the EPR spectrum shows a tetragonally distorted line shape with ($A_{\parallel}$ = 45 G, $g_{\perp}$ = 1.990, $g_{\parallel}$ = 1.955, $g_{average}$ = 1.979; see electronic supporting information). For a square-planar-based Mo complex where the metal is coordinated to the sulfur atoms of mnt and the nitrogen of *o*-aminothiophenol, the fourth corner is presumably occupied by a hydroxido ligand, as shown in Scheme 3. The proton associated with this hydroxido group is positioned in such a way that it interacts with the unpaired electron of Mo^{V} in the d_{xy} orbital. Such super hyperfine splittings generally appear in the 2–7 G range for a Mo^{V}–OH interaction.[17a,17b] In the present case the broad nature of the EPR signal [component line width (peak separation) = 30 G] prevents us from identifying any H-related superhyperfine splitting. The retention of a weak Mo^{V} signal at $<g>$ = 1.999 could be associated with the formation of a side product. This EPR signal also loses its intensity on prolonged standing and finally disappears.

A green tarry product, which is soluble in dichloromethane but not in benzene or toluene, was obtained from the mother liquor after removal of the solvent. This solubility difference suggests that the by-product does not contain a neutral complex with an $\{Mo(NS)_3\}$ core.[17] If this product were to contain a Mo^{V} monomeric tris-chelated by-product like $[Mo^{V}(abt)_3]^{-}$ type complex[17] then the appearance of a more delocalized $<g>$ value near to 2 would be likely and the core of the complex would probably be $\{MoS_6\}$ or $\{Mo(NS)_3\}$, or a combination of these two.[17] Further characterization of this species is currently underway. It is important to note that **2** could only be isolated in good yield after refluxing the reaction mixture for 20 h; shorter reaction times led to the isolation of large amounts of unreacted **1**. These observations can be interpreted as follows. Complex **1** reacts initially with 2-aminothiophenol by opening the oxido-bridged dimeric structure, which results in the

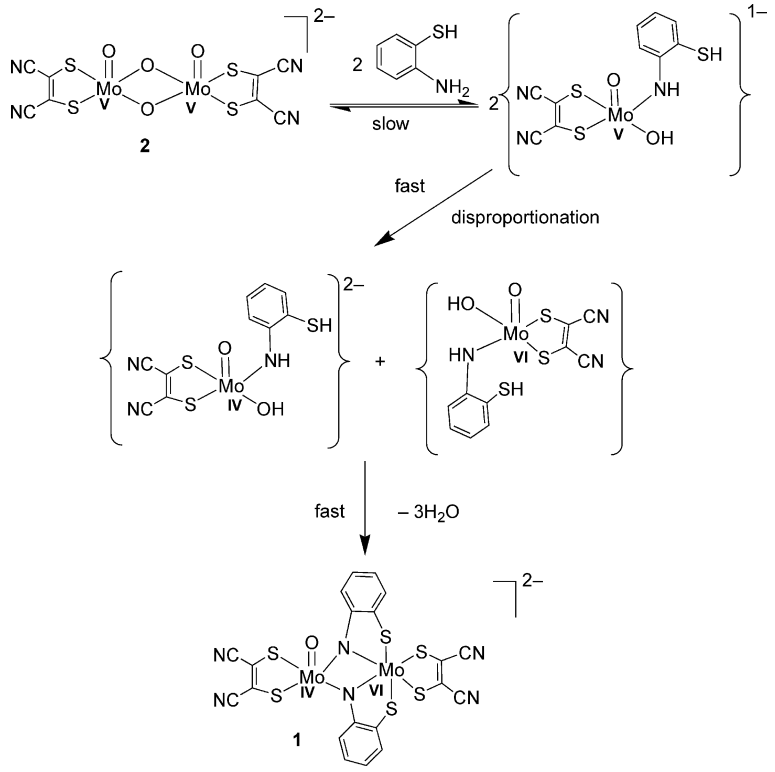

Scheme 3. Proposed mechanism for the formation of $(Bu_4N)_2[Mo^{IV}O(mnt)Mo^{VI}(mnt)\{o\text{-aminobenzothiolato}(3-)\text{-}N,S\}_2]$ (**2**) from the reaction of $(Bu_4N)_2[Mo^{V}_2O_4(mnt)_2]$ (**1**) with 2-aminothiophenol via an EPR-active intermediate species.

appearance of a Mo^V signal and a complex with an $\{Mo^V(O)(S)_2(RNH)(OH)\}$ core, which disproportionates to $\{Mo^{IV}(O)(S)_2\}$ and $\{Mo^{VI}(O)(S)_2\}$ moieties upon heating (Scheme 3). These intermediates interact with the dangling SH groups that result from weak oxido coordination to Mo^{VI}. This leads to complete deprotonation of the RNH^- groups (finally releasing three equivalents of H_2O), which becomes a bridging RN^{2-} (sp^2-hybridized, isoelectronic to O^{2-}) ligand (Scheme 3).

The reaction of **1** with $HSCH_2CH_2NH_2$ in CH_3CN initially gives a green solution, which turns orange upon precipitation of a yellow complex. This complex was identified as $[Mo^{VI}O_2(SCH_2CH_2NH_2)]$ by subsequent comparison with literature data[14] and its formation is accompanied by that of $[Bu_4N]_2[Mo^{IV}O(mnt)_2]$.[3c] Both complexes were isolated in a 1:1 ratio, thus confirming the disproportionation of EPR-active Mo^V into Mo^{IV} and Mo^{VI} species. In this case the absence of a phenyl ring means that there is no π interaction, which may speed up the disproportionation reaction. The discrete monomeric intermediates further rearrange in a ligand-exchange reaction to yield Mo^{IV} monoxido and Mo^{VI} dioxido complexes.[3c]

Structural Descriptions

The structure of **1** has been reported previously.[6a] An ORTEP view of the anion of **2** is shown in Figure 2 and selected bond lengths and angles are listed in Table 2. Compound **1** is a symmetrical dimeric Mo^V complex in which each molybdenum center of the anion of **1** possesses a pentacoordinate square-pyramidal geometry where the basal plane contains two S donor atoms from one mnt ligand and two bridging oxido groups. One terminal oxido group in the axial position completes the square-pyramidal geometry. The Mo atoms lie around 0.73 Å above their respective basal planes (S1–S2–O3–O4 and S3–S4–O3–O4, Figure 2). The two Mo atoms are bonded by a metal–metal σ bond with a relatively short bond length of 2.582 Å. The average Mo–O_t bond lengths are 1.68 Å and the two mnt ligands are nearly symmetrically bonded to two Mo atoms, with a mean Mo–S distance of 2.433 Å.

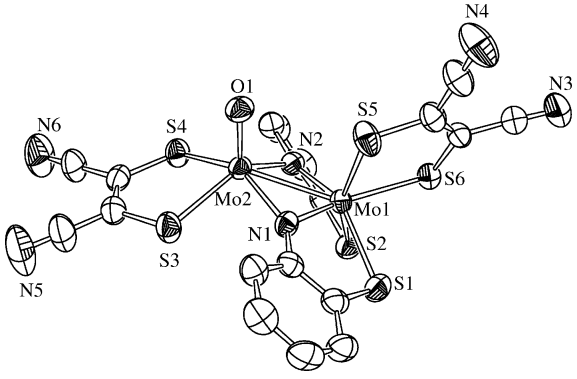

Figure 2. Crystal structure (ORTEP view with 50% thermal ellipsoids) showing the atom numbering scheme (except carbon atoms) for the anion of **2**. Hydrogen atoms have been omitted for clarity.

Table 2. Selected bond lengths and angles for the anion of $(Bu_4N)_2$-$[Mo^{IV}O(mnt)Mo^{VI}(mnt)\{o\text{-aminobenzothiolato}(3^-)\text{-}N,S\}_2]$ (**2**).

Mo(1)–N(1)	1.925(4)	Mo(2)–O(1)	1.681(3)
Mo(1)–N(2)	1.940(4)	Mo(2)–N(1)	2.022(4)
Mo(1)–S(1)	2.4379(16)	Mo(2)–N(2)	2.008(4)
Mo(1)–S(2)	2.4396(15)	Mo(2)–S(3)	2.4170(18)
Mo(1)–S(5)	2.4263(15)	Mo(2)–S(4)	2.4310(14)
Mo(1)–S(6)	2.4786(16)	Mo(1)–Mo(2)	2.6854(11)
N(1)–C(8)	1.386(6)	N(2)–C(6)	1.396(6)
N(1)–Mo(1)–N(2)	95.05(16)	N(1)–Mo(2)–N(2)	90.06(15)
Mo(1)–N(1)–Mo(2)	85.72(16)	Mo(1)–N(2)–Mo(2)	85.70(16)
N(1)–Mo(1)–S(1)	78.21(12)	N(2)–Mo(1)–S(1)	149.40(11)
N(1)–Mo(1)–S(2)	120.14(12)	N(2)–Mo(1)–S(2)	77.63(12)
N(1)–Mo(1)–S(5)	82.56(12)	N(2)–Mo(1)–S(5)	106.27(12)
N(1)–Mo(1)–S(6)	156.70(11)	N(2)–Mo(1)–S(6)	105.25(12)
S(1)–Mo(1)–S(2)	80.18(5)	S(2)–Mo(1)–S(6)	76.20(5)
S(1)–Mo(1)–S(5)	102.43(6)	S(2)–Mo(1)–S(5)	156.92(5)
S(1)–Mo(1)–S(6)	89.47(6)	S(5)–Mo(1)–S(6)	80.88(5)
O(1)–Mo(2)–S(3)	109.29(13)	O(1)–Mo(2)–S(4)	104.33(12)
O(1)–Mo(2)–N(1)	109.56(16)	O(1)–Mo(2)–N(2)	110.26(16)
N(1)–Mo(2)–S(3)	80.84(11)	N(2)–Mo(2)–S(4)	140.21(11)
S(3)–Mo(2)–S(4)	81.87(5)	O(1)–Mo(2)–Mo(1)	109.01(12)

Complex **2** is asymmetric (Figure 2). The asymmetric unit of **2** contains two tetrabutylammonium cations and one anionic dimeric Mo complex. Interestingly, the two Mo centers in **2** have different coordination environments: the first one is a desoxo [Mo(1)] moiety whereas the other [Mo(2)] is an oxidomolybdenum moiety. Mo(1) has a distorted octahedral geometry and is coordinated to three bidentate ligands, whereas Mo(2) has a square-pyramidal geometry with one terminal oxido group at its axial position. The basal plane (N^1–N^2–S^3–S^4) of this square pyramid contains two imido N atoms from an aminothiophenolato ligand and two S atoms from a dithiolene ligand. The Mo(2)–O distance is 1.681 Å. Two metal centers are bridged (denoted by br) by two RN^{2-} (bent imido linkage, Scheme 1) units where each N is in a trigonal planar geometry (sp^2 hybridization) and the average N_{br}–$C_{C_6H_4SN}$ distance is 1.393 Å, which indicates a strong π delocalization of the Mo d electron throughout the benzene ring of the bridging ligand via the bridging N atom. The Mo(2)–N_{br} distances (2.008 and 2.022 Å) are longer than the Mo(1)–N_{br} distances (1.940 and 1.925 Å), which imposes an asymmetry in the bonding at the two metal centers. The choice of the XY coordinate plane for a distorted octahedral geometry or a basal plane for comparison with the basal plane of the Mo(2) center (square-pyramidal geometry) is very difficult for such an asymmetric molecule. However, we can consider that the N_1, N_2, S_1, and S_6 donor atoms contribute to the XY coordinate plane or basal plane in this octahedral geometry due to the metal–metal bond formation. The basal plane of Mo(1) (N_1–N_2–S_1–S_6) makes an angle 26.41° (Figure 3) with the basal plane (XY coordinate plane) of the Mo(2) center (mean plane of the N1, N2, S1, and S6 donor atoms), which is nearly a quarter of 90°. The Mo–Mo bond is somewhat longer (2.685 Å) than that for **1**. The metal–metal bond length in most bridged bimetallic system depends on the size of the bridging atoms and for N atoms it should be shorter than O atoms (Mo–Mo distance is 2.58 Å for **1**), although the reverse is observed here. This is probably due to the overlap of the corresponding σ- and π-bonding orbitals. The Mo–Mo bond lengths in a series of dithiolene-coordinated dimeric Mo complexes are listed in Table 3.

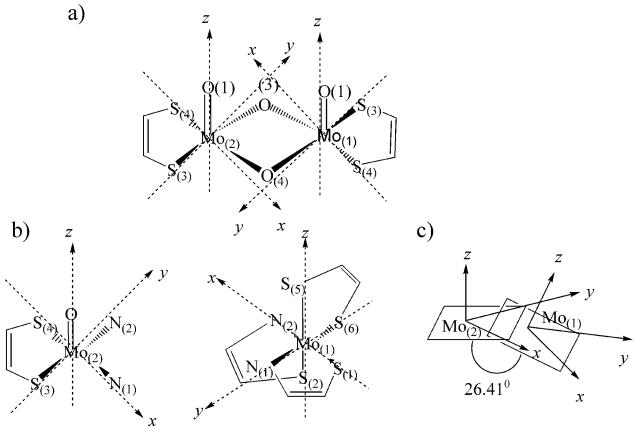

Figure 3. View of the basal plane containing the Mo center in $(Bu_4N)_2[Mo^V_2O_4(mnt)_2]$ (**1**) (a) and $(Bu_4N)_2[Mo^{IV}O(mnt)$-$Mo^{VI}(mnt)\{o\text{-aminobenzothiolato}(3\text{–})\text{-}N,S\}_2]$ (**2**; b and c).

Most dtc-coordinated diimido-bridged dimeric Mo^V complexes with an $\{Mo^V_2O_2(\mu\text{-}NR)_2\}^{2+}$ core are structurally symmetrical[9] like **1**, whereas diimido-bridged dimeric Mo^V complexes like $[Mo^VO(dtc)(\mu_2\text{-}NC_6H_4S)_2Mo^V(dtc)]$[10] are asymmetric. The desoxomolybdenum center in this compex is very close to trigonal prismatic whereas in **2** the

Table 3. Mo–Mo bond lengths of selected mnt-coordinated dimeric Mo complexes.

Complex	Bridging atoms	Mo–Mo [Å]	Ref.
$[Bu_4N]_2[Mo^V_2O_4(mnt)_2]$	O, O	2.581	[6a]
$[Bu_4N]_2[Mo^V_2O_2(mnt)_2(\mu\text{-}O)(\mu\text{-}SPh)(\mu\text{-}Br)]$	O, S_{SPh}	2.670	[6a]
$[Bu_4N]_2[Mo^V_2O_2(mnt)_2(\mu\text{-}O)(\mu\text{-}SPh)(\mu\text{-}CH_3SO_3)]$	O, S_{SPh}	2.730	[6a]
$[Bu_4N]_2[Mo^V_2O_2(mnt)_2(\mu\text{-}O)(\mu\text{-}SEt)(\mu\text{-}CH_3SO_3)]$	O, S_{SEt}	2.731	[6a]
$[Bu_4N][Mo^V_2O_2(mnt)_2(\mu_2\text{-}SPh)_2(\mu\text{-}OMe)]$	S_{SPh}, S_{SPh}	2.856	[6a]
$(Bu_4N)_2[Mo^{IV}O(mnt)Mo^{VI}$ (mnt)$\{o\text{-aminobenzothiolato}(3\text{–})\text{-}N,S\}_2]$	$N_{C_6H_4S}$, $N_{C_6H_4S}$	2.685	this work
$[Mo^V_2O(dtc)_2(\mu_2\text{-}N\text{-}C_6H_4S)_2]$	$N_{C_6H_4S}$, $N_{C_6H_4S}$	2.659	[10a]
$[Mo^V_2O_2(\mu_2\text{-}N\text{-}p\text{-tol})_2(dtc)_2]$	N-*p*-tol, N-*p*-tol	2.629	[9]
$[Mo^V_2O_2(\mu_2\text{-}NPh)_2(dtc)_2]$	NPh, NPh	2.645	[9]
$[Mo^V_2O_2(\mu_2\text{-}N\text{-}C_6H_4Me\text{-}o)_2(dtc)_2]$	N-C_6H_4Me-*o*, N-C_6H_4Me-*o*	2.633	[9]
$[Mo^V_2O_2(N\text{-}C_6H_4Me\text{-}o)_2(\mu_2\text{-}N\text{-}C_6H_4Me\text{-}o)_2(dtc)_2]$	N-C_6H_4Me-*o*, N-C_6H_4Me-*o*	2.632	[9]
$[Mo^V_2O(dtc)_3(\mu_2\text{-}NPh)_2][BF_4]$	NPh, NPh	2.654	[9]

same center adopts a distorted octahedral geometry. This difference is due to the small bite angle of the dtc ligand compared to mnt. The trigonal-prismatic distortion may have a different bonding scheme that does not affect the Mo–Mo bond length as much as in the corresponding symmetric systems. The average Mo–S bond lengths of all these complexes are very similar although the Mo–Mo bond length in **2** is slightly longer (Table 3) than in dtc-coordinated diimido-bridged dimeric Mo^{V} complexes.

Electronic Structure Calculations

The results of the IR and EPR studies and the difference in reactivity of **1** with 1,2-aminothiophenol and 1,2-aminoethanethiol strongly support that compound **2** may possess a mixed-valent $\{M_2\}$ unit. In view of the different nature of the two Mo centers in **2**, we decided to calculate the ground-state electronic structures of **1** and **2** at the DFT (B3LYP) level of theory to determine the energies and compositions of their molecular orbitals (MOs). In both cases the initial geometry was taken from the crystal structure and the geometry was optimized in the gas phase. Additional single-point calculations taking into account a solvent effect were also performed. Selected frontier molecular orbitals, together with their percentage contributions estimated from a Mulliken population analysis calculated in acetonitrile medium, are shown in Figure 4. The assignment of the type of each MO was made on the basis of its composition and by visual inspection of its localized orbital. The coordinate frames for both compounds were assigned by a visual inspection of the d_{z^2} and d_{xy} orbitals and this assignment was found to agree with previous assignments.[7,8] Because of the presence of two different coordinate frames in one molecule that differ from planarity, two additional single-point calculations were carried out using two different coordinate frames (as described in Figure 3) to calculate the percentage contribution of the atomic orbital to the MOs. A table comparing selected bond lengths obtained from the crystal structure and the gas-phase-optimized geometry is given as supporting information. The percentage contributions of the atomic orbitals to selected MOs for **1** and **2** are listed in Table 4.

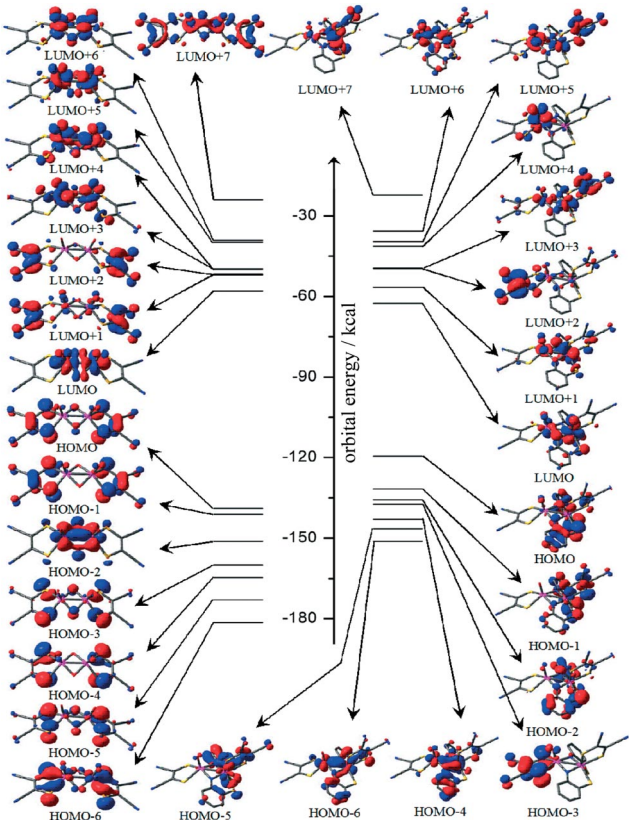

Figure 4. Pictorial representation of the molecular orbitals with levels energy (kcal mol^{-1}; seven highest-occupied and eight lowest-unoccupied) of $(Bu_4N)_2[Mo^{V}_2O_4(mnt)_2]$ (**1**) (left) and $(Bu_4N)_2$-$[Mo^{IV}O(mnt)Mo^{VI}(mnt)\{o\text{-aminobenzothiolato}(3-)\text{-}N,S\}_2]$ (**2**) (right) calculated in acetonitrile.

Figure 4 shows the frontier orbitals of **1** and **2** that control the electronic transitions and electrochemical behaviors of these complexes. The two highest molecular orbitals (HOMO and HOMO–1) for **1** have a large contribution

Table 4. Percentage contributions of atomic orbitals to selected molecular orbitals of $(Bu_4N)_2[Mo^{V}_2O_4(mnt)_2]$ (**1**) and $(Bu_4N)_2[Mo^{IV}O$-$(mnt)Mo^{VI}(mnt)\{o\text{-aminobenzothiolato}(3-)\text{-}N,S\}_2]$ (**2**), calculated in acetonitrile.

MO	1	2
LUMO+7	Ligand π* + metal d_{z^2}	Ligand S π*
LUMO+6	[33% d_{yz} {Mo(1)} + 32% d_{yz} {Mo(2)} + O] π	[33% d_{xz} {Mo(1)} +29% d_{xz} {Mo(2)}] π
LUMO+5	[37% d_{xz} {Mo(1)} + 38% d_{xz} {Mo(2)} + O] π	[25% d_{z^2} {Mo(2)} + ligand] π*
LUMO+4	[36% d_{yz} {Mo(1)} + 35% d_{xz} {Mo(2)} + O] π	[56% d_{yz} {Mo(2)} + Pz (O)] π*
LUMO+3	[32% d_{xy} {Mo(1)} + 32% d_{xy} {Mo(2)} + O] π	[20% d_{xy} {Mo(1)} + 12% d_{xy} {Mo(2)}] σ* + ligand π
LUMO+2	(N≡C–C=C–C≡N) π* of mnt	(N≡C–C=C–C≡N) π* of mnt
LUMO+1	(N≡C–C=C–C≡N) π* of mnt	[38% d_{xz} {Mo(1)} + 14% d_{xy} {Mo(2)}] σ* + ligand π
LUMO	[32% d_{xy} {Mo(1)} + 32% d_{xy} {Mo(2)}] σ*+ O π*	[50% d_{yz} {Mo(1)} + 9% d_{xy} {Mo(2)}] σ* + ligand π
HOMO	(S–C=C–S) π*	Sπ of mnt and aminothiophenolate at Mo(1)
HOMO–1	(S–C=C–S) π*	(S–C=C–S) π* of mnt + S π of aminothiophenolate at Mo(1)
HOMO–2	[38% d_{xy} {Mo(1)} + 38% d_{xy} {Mo(2)}] σ + O π	(S–C=C–S) π* of mnt at Mo(2)
HOMO–3	S π* mnt + O π* of bridge oxido	S π of aminothiophenolate at Mo(2)
HOMO–4	S π* of mnt	[10% d_{xy} {Mo(1)} + 6% d_{xz} {Mo(1)} + 5% d_{yz} {Mo(1)} + 18% d_{xy} {Mo(2)}] σ
HOMO–5	S π* of mnt	(S–C=C–S) π* of mnt + S π of aminothiophenolate + C=C π* at Mo(1)
HOMO–6	S π* of mnt	(S–C=C–S) π* of mnt + S π of aminothiophenolate + C=C π* at Mo(1)

from the π* antibonding orbital of the dithiolene ligands (mnt). The next lowest lying and deeply buried occupied orbital (HOMO–2) is formed from a σ-bonding interaction between the d_{xy} orbitals of two Mo centers (each with 32%) and the O π orbital of the bridging oxygen atoms. HOMO–3 to HOMO–6 have only a π orbital contribution from the S atoms of two dithiolene ligands. The LUMO is formed from an antibonding interaction between the d_{xy} orbitals of two Mo centers (38% each) and the O π orbitals of the bridging oxygen atoms. The next two highest energy virtual orbitals (LUMO+1 and LUMO+2) have contributions from the C–CN π antibonding orbital of mnt. The rest of the metal d orbitals involved in lateral π overlap are empty and in a high energy state. The Mo–Mo σ bond of most symmetric dimeric di-μ_2-oxido Mo^V (d^1 system) complexes is formed by the head-on overlap of the d_{xy} orbitals of each Mo center. This is also the case for complex **1**, where the HOMO–2 and LUMO correspond to the σ bonding and antibonding molecular orbitals, respectively, and are formed by the usual overlap of two d_{xy} orbitals from each metal center.

The situation for **2** is somewhat more complicated because of its unsymmetrical nature and the fact that the two metal centers have different geometries. These metals are bridged by an RN^{2-} anion and hence should have different bonding. The HOMO, HOMO–1, and HOMO–2 are ligand (mnt and 2-aminothiophenolate) S π based orbitals, and a deeply buried HOMO–4 shows the bonding interaction between the two Mo centers, which originated from the overlap of the d_{xy} orbital of Mo(2) (18%) and a mixture of three d orbitals (d_{xy}, d_{xz}, and d_{yz}) of Mo(1) (8%, 6%, and 5% respectively; Table 4). The total contribution of the metal d orbitals is 37%. The higher energy LUMO, LUMO+1, and LUMO+3 (Figure 4, Table 4) show antibonding interactions with Mo(2) (d_{xy}) and Mo(1) (d_{xy}, d_{yz}, and d_{xz}), whereas LUMO+2 has a maximum contribution from the N≡C–C=C–C≡N π* antibonding orbital. Based on the total metal contribution to HOMO–4 the extent of bonding for the σ bond is 37%, and based on the full contribution of the Mo(2) (d_{xy}) orbital (considering only a σ-bonding interaction between the two metal centers), the extent of σ-bonding overlap of the d_{xy}, d_{yz}, and d_{xz} orbitals of Mo(1) is approximately 50, 25, and 25% respectively.

Cotton and co-workers[18] have established the formation of a maximum of four M–M bonds (σ, 2π, δ) for any $\{M_2\}$ unit where both the metal centers contribute atomic orbitals of the same symmetry to give maximum overlap and form a particular metal–metal bond, although the possible formation of five M–M bonds has also been reported recently.[19] The formation of an M→M′ dative bond with different orbitals (Md_{z^2}, $M'd_{x^2-y^2}$) in heterobimetallic systems involves the *xy*-coordination frame of the respective metal center as orthogonal to each other.[20] The complex $[Mo_2(O\textit{i}Pr)_4(dmpe)_2]$ is an interesting example with dissimilar coordination of two metal centers.[21] The strength of the multiple Mo–Mo bonds in this complex is maximum for a perfectly eclipsed configuration of the basal planes and tends to zero for a fully staggered configuration. This has been related to the extent of π and δ overlap, which is itself dependent on the twist angle.[22] However, the situation may differ for a σ bond when the angle between the basal planes of the two metal centers is about one quarter of 90°, as we observed for **2**. None of the five d orbitals of a metal center in the $\{M_2\}$ moiety can be transformed to another center by rotating the coordinate frame by an angle of one quarter of 90°. This deviation from planarity of the coordination framework of two metal centers will minimize the extent of overlap of their respective d orbitals. This deviation is 26.41° for complex **2**, which forbids a perfect σ overlap between the Mo(2) d_{xy} and Mo(1) d_{xy} orbitals. However, a partial symmetry is allowed for the overlap of Mo(2) (d_{xy}) and Mo(1) (d_{xy}, d_{yz}, d_{xz}) orbitals for a direct Mo–Mo interaction where the two bonding electrons come from $Mo(2)^{IV}$ (MO energy level diagram shown in Figure 3). The extent of bonding is only about 35% accounted for by σ donation from a metal d orbital, therefore the Mo–Mo distance is longer then expected (according to the size of the bridging atom). This bond also involves some degree of π interaction, as reflected by the Mo(1)–N_{br} bond length being shorter than Mo(2)–N_{br} and high delocalization of the metal centers with the ligand π orbitals throughout the molecule. Thus, the interaction of two asymmetric metal center fragments can be viewed as a donor–acceptor interaction where partial σ overlap between one donor and three acceptor orbitals (or a hybrid of three metal d orbitals) as well as a π (ligand) donor/acceptor interaction supplement the resulting bond; this explains the diamagnetism of **2**. Under such circumstances, it is difficult to assign the exact oxidation states of the two Mo centers in **2**, although assigning the formal oxidation state of Mo(1) center as +6 and the Mo(2) center as +4 is a good approximation that solves the problem of electron bookkeeping and supports the experimental results.

A population analysis (Mulliken and NBO) of the partial atomic charges for complexes **1** and **2** was carried out using the same method and basis set. The partial atomic charge distributions of selected atoms are listed in Table 5. The overall charge distribution is symmetric in **1** and asymmetric in **2**. The atomic charge distribution of the S atoms is nearly zero for both **1** and **2**, and the N and O atoms both

Table 5. Calculated gas-phase Mulliken and NBO atomic charges of the $\{Mo_2O_4S_6\}^{2-}$ core of **1** and the $\{Mo_2N_2S_6O\}^{2-}$ core of **2**.

	1		**2**	
Atom	Mulliken	NBO	Mulliken	NBO
Mo(1)	0.62	1.14	0.13	0.35
Mo(2)	0.62	1.14	0.59	0.96
S1	0.16	–0.09	0.23	–0.01
S2	0.16	–0.09	0.27	0.01
S3	0.16	–0.09	0.19	0.08
S4	0.16	–0.09	0.20	0.06
S5	–	–	0.33	0.07
S6	–	–	0.34	0.01
O1	–0.44	–0.52	–0.44	–0.49
O2	–0.44	–0.52	–	–
N1/O3	–0.62	–0.72	–0.86	–0.58
N2/O4	–0.62	–0.72	–0.83	–0.58

carry negative charges. The two Mo centers in **1** have the same positive atomic partial charges whereas the charge distribution at the two metal centers in **2** is unequal and is lower than **1** [Mulliken for **2** Mo(1): 0.13, Mo(2): 0.59; NBO Mo(1): 0.35, Mo(2): 0.96]. Although the formal oxidation state of Mo(2) is +4, which is less than that (+6) of Mo(1), the Mo(2) center has a greater positive charge. This may be due to the presence of a highly electron-withdrawing Mo=O moiety at Mo(2). Similarly, the presence of all-thiol ligation in Mo(1) clearly reflects the high delocalization of the ligand π orbitals, which reduces its positive atomic partial charge.

Cyclic Voltammetry

The cyclic voltammograms (CVs) of **1** (Figure 5) and **2** (Figure 6) were recorded in a 10^{-3} M solution in acetonitrile at 298 K at a scan rate of 100 mV s^{-1}. The potential was measured using a glassy carbon electrode with Ag/AgCl as reference electrode with 0.1 M tetrabutylammonium perchlorate as supporting electrolyte. The CV of **1** shows one irreversible oxidation at 1.22 V and one quasi-reversible reduction at –1.56 V. The CV of **2** shows two irreversible ligand oxidations at 0.85 and 1.08 V and a fully reversible reduction at –1.16 V.

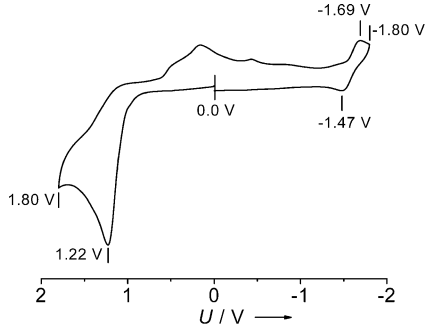

Figure 5. Cyclic voltammogram of $(Bu_4N)_2[Mo^V_2O_4(mnt)_2]$ (**1**) in acetonitrile. Scan rate: 100 mV s^{-1}, *U* stands for voltage.

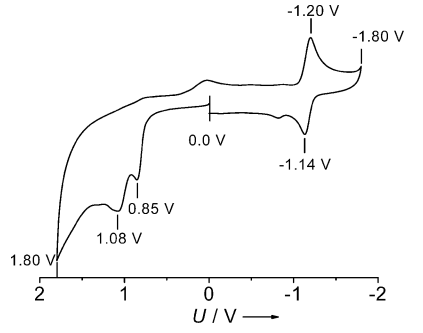

Figure 6. Cyclic voltammogram of $(Bu_4N)_2[Mo^{IV}O(mnt)$-$Mo^{VI}(mnt)\{o$-aminobenzothiolato(3–)-*N*,*S*$\}_2]$ (**2**) in acetonitrile. Scan rate: 100 mV s^{-1}, *U* stands for voltage.

The CV responses can easily be explained by the nature of the HOMOs and LUMOs. Thus, the irreversible oxidation of **1** is due to oxidation of the mnt ligand because the HOMO of **1** is a ligand S π* orbital of mnt. The two irreversible oxidations observed for **2** are associated with two types of ligand oxidation because the HOMO, as the potential electron donor, is predominately populated by the S π* orbitals of mnt and the 2-aminothiophenolato ligand. The quasi-reversible reduction of one of the Mo^V centers is viewed as the population of an electron on the LUMO, which is formed by the antibonding interaction of two metal d_{xy} orbitals. In the LUMO of **2** the Mo(2) d_{xz} orbital is predominantly populated and a fully reversible reduction of Mo^{VI} center is possible. This reversibility clearly indicates that the one-electron reduction of **2** does not significantly affect the Mo–Mo bond because of the high delocalization by σ donation and π acceptance through the bridging ligands between the two Mo centers of the respective fragments and also through the benzene rings of the bridging ligands. The one-electron reduction of **1** makes this system unstable because the addition of this electron to the σ* antibonding orbital reduces the bond order and directly affects the Mo–Mo bond. The less negative potential for reduction of the Mo center of **2** compared to **1** correlates nicely with the smaller HOMO–LUMO gap found for **2** by the DFT calculations.

Optical Absorption Spectra

The electronic spectra of complexes **1** and **2** were recorded in acetonitrile. Complex **1** shows only one peak at 353 nm, whereas complex **2** shows two peaks at 338 and 439 nm in the UV region. Two other low energy bands observed for **2** in the visible region at around 580 and 648 nm, with almost equal intensity, are absent in **1**. The absorption spectra of **1** and **2** are shown in Figure 7. The metal-mnt complexes and the free Na_2mnt ligand show an absorption band at around 364 nm due to an intraligand charge-transfer transition. The electronic spectra of complexes **1** and **2** were also measured in other solvents with different polarities (dichloromethane and dmf; see electronic supporting information). No remarkable changes in the position of the maximum absorption wavelength (λ_{max}), the optical absorption coefficient, or the overall nature of the absorption spectra of **1** and **2** were observed on changing the solvent polarity.

TD-DFT calculations on **1**, **2**, and the free ligand $[\{S_2C_2(CN)_2\}^{2-}]$ were carried out at the G03/B3LYP level in the gas phase and with a solvent effect (COSMO) on the gas phase optimized geometry to assign the experimentally observed low-lying electronic transitions in the visible region. The time-dependent DFT approach (TD-DFT) is a rigorous method for calculating vertical electronic excitation spectra. The solvent dielectric constant and radius were considered as being those of acetonitrile. The free mnt ion is not soluble in acetonitrile and its experimental spectrum was therefore recorded in methanol, thus the solvent effect was calculated for the solvents acetonitrile and methanol. Singlet excited states were calculated based on the singlet ground-state geometry. The lowest 40 singlet excited states with oscillator strengths greater than 0.01 ($f > 0{:}01$)

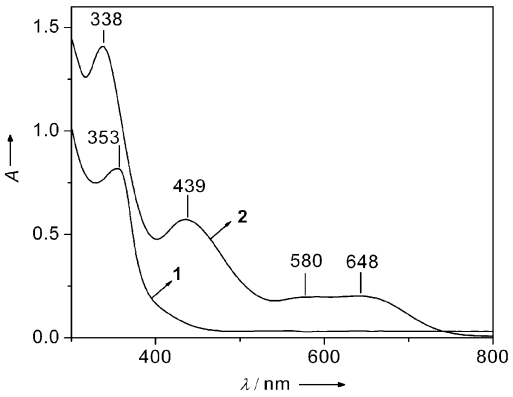

Figure 7. Electronic absorption spectrum of a 5×10^{-5} M solution of $(Bu_4N)_2[Mo^V_2O_4(mnt)_2]$ (**1**) and $(Bu_4N)_2[Mo^{IV}O(mnt)Mo^{VI}(mnt)\{o\text{-aminobenzothiolato}(3-)\text{-}N,S\}_2]$ (**2**) in acetonitrile.

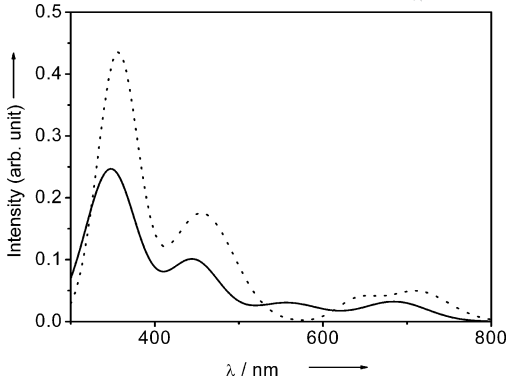

Figure 9. Computed absorption spectrum of $(Bu_4N)_2[Mo^{IV}O(mnt)\text{-}Mo^{VI}(mnt)\{o\text{-aminobenzothiolato}(3-)\text{-}N,S\}_2]$ (**2**) in the gas phase (solid line) and in acetonitrile (dotted line).

were considered for TD-DFT calculations, and the singlet excited states were fitted to Gaussian line shapes. The simulated CT spectra were prepared by fitting each excited state energy to a Gaussian curve with a full-width-at-half-maximum of 45 nm for complex **1** and 63 nm for complex **2**. A table containing the low-energy excitation wavelengths and oscillator strengths (OS) for compounds **1**, **2**, and the free ligand in the gas phase and in acetonitrile is provided as supporting information. The computed electronic spectra of **1** and **2** in the gas phase and in acetonitrile are shown in Figures 8 and 9 respectively. According to the TD-DFT calculations the free ligand mnt has only one absorption band in the visible region at around 427 nm in the gas phase and around 415 nm in both solvents. The calculated band in these three different media shows a blue shift with respect to the experimental value (approx. 364 nm) and this band is due to the intraligand charge transfer from S–C=C–S π* (HOMO) to NC–C=C–CN (LUMO) π*.

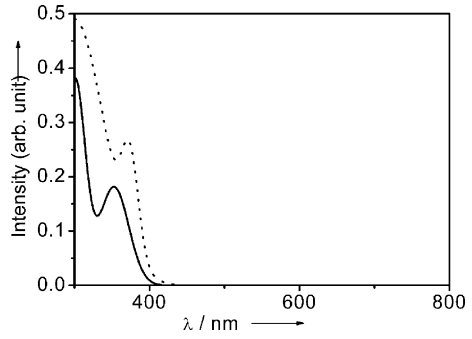

Figure 8. Computed absorption spectrum of $(Bu_4N)_2[Mo^V_2O_4(mnt)_2]$ (**1**) in the gas phase (solid line) and in acetonitrile (dotted line).

One intense charge-transfer band was found at 368 nm in the gas phase and at 370 nm in the solvent phase for complex **1**. The experimentally observed peak at 364 nm can be assigned as either a ligand S–C=C–S π* (HOMO) to ligand NC–C=C–CN (LUMO+3) internal charge-transfer transition or an intraligand charge-transfer transition. Another high energy charge-transfer band was computed in the lower UV region. This is responsible for the higher energy transition ($\lambda < 300$, experimentally observed) which is due to an MLCT transition from HOMO–2 to LUMO+6. Unfortunately, the solvent absorption prevented us from recording the experimental absorption spectrum in the region below 300 nm.

The single electron in the d_{xy} (Mo^V) orbital, which is engaged in metal–metal bond formation, is deeply buried and does not take part in any electronic transition in the visible region, although it does appear in the very high energy region ($\lambda < 300$). The other empty d orbitals are highly destabilized by π interactions and this may be the reason why **1** does not show any MLCT or LMCT transition in the 300–1000-nm region.

The most intense absorption bands at 335 nm in the gas phase and 342 nm in the solvent phase for **2** match well with the experimentally observed absorption band at 338 nm. This can be assigned as the sum of major overlapping HOMO–2 to LUMO+5 and LUMO+6, HOMO–5 to LUMO+3, and HOMO–5 to LUMO+3 electronic transitions with ligand S π to metal d orbital charge transfer character (LMCT). The second LMCT band is at 429 nm in the gas phase and at 451 nm in the solvent phase in the visible region, which is compatible with the experimentally found absorption at 439 nm. There are also some slightly lower intensity transitions found within ±30 nm of the 439 nm band. The experimentally observed band at 439 nm can therefore be assigned as a multiple LMCT band originating from different types of ligand S π* antibonding orbital to metal antibonding d orbital transitions. Because of the multiple nature of the charge-transfer transitions appearing in a very close region, this absorption is broad in nature and its half width is larger than that of the peak at 338 nm. The two experimentally observed low energy and less intense peaks around 648 and 580 nm are broad in nature. The calculated absorption peaks found in this region at three different wavelengths (683, 617, and 549 nm) in the gas phase are shifted to 705, 636, and 554 nm, respectively, in the solvent phase and have almost the same intensity. These three peaks give rise to two absorptions at 683 and

at 558 nm in the gas phase and at 705 and at 563 nm in the solvent phase, respectively. Thus, the experimentally found peak at 580 nm is due to a charge-transfer transition from two different types of ligand S π* antibonding orbitals to metal antibonding d orbitals (HOMO to LUMO+1 and HOMO–1 to LUMO). The peak at 648 nm (experimental) can be assigned as a ligand S π orbital to metal antibonding d orbital (HOMO to LUMO) transition. The simulated spectra of **1** and **2** show a shift of the wavelength of some charge-transfer bands between the solvent model and the gas phase, although the experimental absorption spectra recorded in solvents with different polarities show no such shifts.

Conclusions

Most known higher valent (+4, +5, and +6) dimeric Mo complexes are symmetrical with respect to the two molybdenum centers, therefore complex **2** is unique in that it features one oxido and one desoxo Mo moiety bridged by a common ligand that imparts a different coordination framework around each Mo center. Such structural asymmetry, the presence of an Mo–Mo bond between the two Mo centers, extended π delocalization throughout the molecule, the position of the $\nu_{(Mo=O)}$ absorption, and a detailed EPR study support the presence of a mixed-valent $\{Mo_2(RN)_2\}$ unit in **2**. The individual Mo centers [Mo(1) and Mo(2)] in **2** may have nearly +6 and +6 oxidation states. The redox chemistry observed in the CVs for both **1** and **2** has been correlated with the theoretical results, and the observed electronic absorption spectra have been analyzed by TD-DFT calculations. Analysis of the bonding by DFT calculations has shown a new bonding feature in the asymmetric dimeric complex **2**. The plausibility of a σ-type overlap involving one d orbital from one metal center and a hybrid orbital of three d orbitals from the other metal center in a dimeric molecule has been investigated in a situation where the deviation of the angle between the respective basal planes is around 26°. While checking such a possibility the overlap of one donor metal d orbital and three acceptor metal d orbitals to form a molybdenum–molybdenum bond is invoked. The possibility of influencing such bonding by changing the donor or the acceptor is currently being explored.

Experimental Section

Starting Materials and Physical Methods: All reactions were carried out in air and under ambient conditions. Bu_4NBr, 2-aminothiophenol, and 2-aminoethanethiol were obtained from Aldrich and NaCN and ammonium heptamolybdate from S. D. Fine chemicals Ltd. India. $Na_2[S_2C_2(CN)_2]$ (Na_2mnt) was prepared according to a literature method.[12] Solvents and reagents were distilled and dried by standard procedures. IR spectra were recorded as CsI pellets with a Bruker Vertex 70 FT-IR spectrophotometer. Elemental analyses for carbon, hydrogen, nitrogen, and sulfur were obtained with a Perkin–Elmer 2400 microanalyser. Electronic spectra were recorded with a Cintra 10 UV/Vis spectrophotometer. Low-temperature (frozen state, 77 K) EPR spectra were recorded with a Varian E-109 (X-band) spectrometer in dual cavity mode and the EPR parameters were calculated from the measured spectra using DPPH (g = 2.0023) as calibrant. Room-temperature solution spectra were recorded with a Bruker EMX X-band EPR spectrometer using DPPH (g = 2.0023) as calibrant and the EPR parameters were calculated using the Bruker WINEPR system. Samples for room-temperature solution EPR spectra were prepared under argon and then transferred into a flat quartz cell fitted with a gas-tight septum. Cyclic voltammetric measurements were performed with a BASi Epsilon-EC Bioanalytical systems, Inc. instrument. Cyclic voltammograms of 10^{-3} M acetonitrile solutions of the compounds were recorded with a glassy carbon working electrode and 0.1 M Bu_4NClO_4 as supporting electrolyte; all experiments employed an Ag/AgCl reference electrode and platinum auxiliary electrode. All electrochemical experiments were performed under argon at 298 K.

Synthesis of $(Bu_4N)_2[Mo^{IV}O(mnt)Mo^{VI}(mnt)\{o$-aminobenzothiolato-(3–)-*N*,*S*$\}_2]$ (2): $(Bu_4N)_2[Mo_2O_4(mnt)_2]$ (1020 mg, 1 mmol) was dissolved in 15 mL of dry acetonitrile and 2-aminothiophenol (2 mL, 2 mmol) was added dropwise with constant stirring, whereupon the color of the solution changed from yellow to bright green. The mixture was refluxed for 6–8 h, after which time the color of the solution had changed to dark green. The reaction mixture was cooled to room temperature. A microcrystalline product was isolated directly from this solution upon addition of 2-propanol and diethyl ether (840.0 mg 69%). The compound was recrystallized from acetonitrile, 2-propanol and diethyl ether. $C_{52}H_{80}Mo_2N_8OS_6$ (1217.54): calcd. C 51.53, H, 6.58, N 9.21, S, 15.78; found C 51.48, H 6.82, N 9.35, S 15.75. FT-IR (CsI): $\tilde{\nu}$ = 939 cm^{-1} (vs, Mo=O). UV/Vis: $\lambda_{CH_2Cl_2}$ (ε) = 338 nm (22659 $M^{-1}cm^{-1}$), 439 (10819), 586 (3713), 645 (3796).

Reaction of $(Bu_4N)_2[Mo_2O_4(mnt)_2]$ with $HSCH_2CH_2NH_2$: $(Bu_4N)_2[Mo_2O_4(mnt)_2]$ (1020 mg, 1 mmol) was dissolved in 15 mL of dry acetonitrile then a solution of 2-aminoethanethiol (0.16 g, 2 mmol) in 5 mL of methanol was added with constant starring, whereupon the color of the solution changed from yellow to dark orange and finally to brownish green with precipitation of an orange solid. The reaction mixture was allowed to stand for a few hours to complete the precipitation and was then filtered. The filtrate was washed with 2-propanol and finally with diethyl ether and dried under vacuum (A; 408 mg, 46%). Addition of 2-propanol and diethyl ether to the filtrate resulted in the precipitation a dark-green crystalline product, which was washed with 2-propanol and diethyl ether and dried under vacuum (B; 134 mg, 48%).

Analysis for A: The analytical and spectrochemical data were identical to those for $[Bu_4N]_2[Mo^{IV}O(mnt)_2]$.[3c]

Analysis for B: The analytical and spectrochemical data were identical to those for $[Mo^{VI}O_2(SCH_2CH_2NH_2)]$.[14]

X-ray Structure Determination: Suitable crystals of $(Bu_4N)_2[Mo^{IV}O(mnt)Mo^{VI}(mnt)\{o$-aminobenzothiolato(3–)-*N*,*S*$\}_2]$ (**2**) were obtained from the crystallization procedures described in the synthesis. A single crystal of **2** was glued to a glass fiber and mounted on a Bruker Smart Apex diffractometer equipped with a CCD area detector and data were collected using graphite-monochromated Mo-K_α radiation (λ = 0.71069 Å) at low temperature (100 K). An empirical absorption correction was applied using the SADABS program. Cell constants were obtained from the least-squares refinement of three-dimensional centroids by recording narrow ω rotation frames until completion of almost all reciprocal space in the stated θ range. The data were collected with SMART 5.628 (Bruker, 2003), and were integrated with the Bruker SAINT

program. A total of 20591 reflections were collected (θ = 1.91 to 28.41°), of which 14704 reflections were unique {R_{int} = 0.0320 [$I > 2\sigma(I)$]}. The space group of this compound was determined based on the lack of systematic absences and intensity statistics. The structure was solved using SIR97[23] and refined using SHELXL-97[24] in the space group $P\bar{1}$. Full-matrix least-squares/difference Fourier cycles were performed to locate the remaining non-hydrogen atoms. All non-hydrogen atoms were refined with anisotropic displacement parameters. The final R factor was 6.81% ($wR2$ = 13.30%). Some of carbon atoms of the butyl group of one of the tetrabutylammonium cation were found to be disordered over two positions and were refined with the free part instruction using SHELXL-97. The crystal structure was produced with ORTEP.[25] Selected crystallographic data parameters for **2** are listed in Table 6.

Table 6. Crystallographic data parameters of $(Bu_4N)_2[Mo^{IV}O(mnt)Mo^{VI}(mnt)\{o\text{-aminobenzothiolato}(3-)\text{-}N,S\}_2]$ (**2**).

Empirical formula	$C_{52}H_{80}Mo_2N_8OS_6$
Formula weight	1217.54
Crystal system	triclinic
Space group	$P\bar{1}$
Temperature [K]	100
Z	2
a [Å]	11.258(5)
b [Å]	12.616(5)
c [Å]	22.559(5)
α [°]	85.984(5)
β [°]	76.962(5)
γ [°]	80.766
V [Å^3]	3079(2)
D_{calcd} [Mg m^{-3}]	1.313
$F(000)$	1272
Absorption [mm^{-1}]	0.651
Theta range [°]	1.9–28.41
Reflections collected	20591
Reflections unique	14704
GOF (F^2)	0.993
R_1[a] (wR_2[b])	0.068 (0.1330)

[a] $R_1 = \Sigma||F_o| - |F_c||/\Sigma|F_o|$. [b] $wR_2 = \{\Sigma[w(F_o^2 - F_c^2)^2]/\Sigma[w(F_o^2)^2]\}^{1/2}$.

CCDC-274974 (for **2**) contains the supplementary crystallographic data for this paper. These data can be obtained free of charge from The Cambridge Crystallographic Data Center via www.ccdc.cam.ac.uk/data_request/cif.

Computational Details: All calculations were performed with the Gaussian 03 package (revision B.04).[26] Molecular orbitals were visualized using Gauss View. Geometry optimizations, single point calculations, and population analysis of the molecular orbitals were carried out at the density functional theory (DFT) level with Becke's three-parameter hybrid exchange functional,[27] the non-local correlation provided by the Lee, Yang, and Parr expression, and the Vosko, Wilk, and Nuair 1980 correlation functional (III) local (B3LYP) 6-31g*+ basis set[28] were used for H, C, N, O, and S atoms. The LANL2DZ[29] basis set and LANL2 pseudo-potentials of Hay and Wadt[30] were used for the Mo atom. The initial geometry of the anions of **1** and **2** were taken from the crystal structure[6a] and each geometry was optimized without any symmetry constraints. The initial geometry of the $[S_2C_2(CN)_2]^{2-}$ (mnt^{2-}) was modeled using the same geometrical parameters as in the Mo complex. The optimized minima were characterized by harmonic vibration frequency calculations where minima have no imaginary frequency. For the medium effect, additional single-point energy calculations and time-dependent DFT (TD-DFT) calculations were carried out on the gas phase optimized geometries with the same method, same basis set, and the conductor like screening model[31] (COSMO). The solvent chosen was acetonitrile. The lowest 40 singlet excited states were considered for TD-DFT calculations.

Supporting Information (see also the footnote on the first page of this article): Table showing a comparison of selected bond lengths obtained from the crystal structure and gas-phase optimized geometry; experimental and computed UV/Vis absorption spectra; the HOMO and LUMO of $[S_2C_2(CN)_2]^{2-}$; a table containing low-energy excitation wavelengths and oscillator strengths (OS) for **1**, **2** and $[S_2C_2(CN)_2]^{2-}$; and EPR spectra.

Acknowledgments

Thanks are due to Council of Scientific and Industrial Research (CSIR) for providing a doctoral fellowship (to K. P.) and to the Department of Science and Technology (DST), New Delhi for funding.

[1] a) K. V. Rajagopalan, in *Molybdenum and Molybdenum-Containing Enzymes*, 1st ed. (Ed.: M. P. Coughlan), Pergamon Press, Oxford, **1980**; b) R. S. Pilato, E. I. Stiefel, in *Bioinorganic Catalysis*, 2nd ed. (Eds.: J. Reedijk, E. Bouwman), Marcel Dekker, New York, **1999**, pp. 81–152; c) M. Dixon, E. C. Webb, C. J. R. Throne, K. F. Tipton, *Enzymes*, 3rd ed., Academic Press, New York, **1979**.

[2] E. I. Stiefel, *Dithiolene Chemistry*, in *Progress in Inorganic Chemistry* (Ed.: K. D. Karlin), John Wiley & Sons, New York, **2004**, vol. 52.

[3] a) E. I. Stiefel, *Prog. Inorg. Chem.* **1977**, *22*, 1–223; b) E. I. Stiefel, *Molybdenum(VI)*, in *Comprehensive Coordination Chemistry* (Eds.: G. Wilkinson, R. D. Gillard, J. A. McCleverty), Pergamon, Oxford, **1987**, pp. 1375–1420; c) C. G. Young, *Molybdenum*, in *Comprehensive Coordination Chemistry II* (Eds.: J. A. McCleverty, T. J. Meyer, A. G. Wedd), Pergamon, Oxford, pp. 444–445; d) S. K. Das, P. K. Chaudhury, D. Biswas, S. Sarkar, *J. Am. Chem. Soc.* **1994**, *116*, 9061; e) B. S. Lim, M. W. Willer, M. Miao, R. H. Holm, *J. Am. Chem. Soc.* **2001**, *123*, 8343; f) N. Ueyama, H. Oku, M. Kondo, T. A. Okamura, N. Yoshinaga, A. Nakamura, *Inorg. Chem.* **1996**, *35*, 643; g) J. P. Donahue, C. R. Goldsmith, U. Nadiminti, R. H. Holm, *J. Am. Chem. Soc.* **1998**, *120*, 12869.

[4] a) C. D. Garner, J. M. Charnock, *Molybdenum(IV)*, in *Comprehensive Coordination Chemistry* (Eds.: G. Wilkinson, R. D. Gillard, J. A. McCleverty), Pergamon, Oxford, **1987**, pp. 1329–1374; b) C. G. Young, *Molybdenum*, in *Comprehensive Coordination Chemistry II* (Eds.: J. A. McCleverty, T. J. Meyer, A. G. Wedd), Pergamon, Oxford, **1987**, pp. 470–471; c) J. H. Enemark, J. A. J. Cooney, J.-J. Wang, R. H. Holm, *Chem. Rev.* **2004**, *104*, 1175–1200; d) H. Sugimoto, K. Sieren, H. Tsukube, K. Tanaka, *Eur. J. Inorg. Chem.* **2003**, *14*, 2633–2638.

[5] a) C. D. Garner, J. M. Charnock, *Molybdenum(III), (IV), and (V)*, in *Comprehensive Coordination Chemistry II* (Eds.: G. Wilkinson, R. D. Gillard, J. A. McCleverty), Pergamon, Oxford, **1987**, pp. 1329–1374; b) D. Coucouvanis, *Adv. Inorg. Chem.* **1998**, *45*, 1–73; c) C. G. Young, I. P. McInerney, M. A. Bruck, J. H. Enemark, *Inorg. Chem.* **1990**, *29*, 412–416; d) K. Nagrajan, H. K. Joshi, P. K. Chaudhuri, K. Pal, J. A. Cooney, J. H. Enemark, S. Sarkar, *Inorg. Chem.* **2004**, *43*, 4532–4533; e) A. Majumdar, K. Pal, S. Sarkar, *J. Am. Chem. Soc.* **2006**, *128*, 4196–4197; f) B. S. Lim, R. H. Holm, *J. Am. Chem. Soc.* **2001**, *123*, 1920–1930; g) K.-M. Sung, R. H. Holm, *J. Am. Chem. Soc.* **2001**, *123*, 1931–1943; h) B. S. Lim, J. P. Donahue, R. H. Holm, *Inorg. Chem.* **2000**, *39*, 263–273; i) B. S. Lim, K.-M. Sung, R. H. Holm, *J. Am. Chem. Soc.* **2000**, *122*, 7410–7411; j) J. Jiang, R. H. Holm, *Inorg. Chem.* **2004**, *43*, 1302–1310; k) K.-M. Sung, R. H. Holm, *Inorg. Chem.* **2000**, *39*, 1275–1281.

[6] a) K. Pal, R. Maiti, P. K. Chaudhury, S. Sarkar, *Inorg. Chim. Acta* **2007**, *360*, 2721–2733; b) L. Richard, C. Martin, R. Wiest, *Inorg. Chem.* **1975**, *14*, 2300; c) F. A. Cotton, W. H. Ilsley, *Inorg. Chim. Acta* **1982**, *59*, 213; d) M. G. B. Drew, A. Kay, *J. Chem. Soc. A* **1971**, *89*, 1846; e) V. R. Ott, D. S. Swieter, F. A. Schultz, *Inorg. Chem.* **1977**, *16*, 2538; f) F. A. Schultz, V. R. Ott, D. S. Rolison, D. C. Bravard, J. W. McDonald, W. E. Newton, *Inorg. Chem.* **1978**, *17*, 1758.
[7] a) F. A. Cotton, *Inorg. Chem.* **1965**, *4*, 334; b) F. A. Cotton, *J. Less Common Met.* **1977**, *54*, 3.
[8] A. B. Blake, F. A. Cotton, J. S. Wood, *J. Am. Chem. Soc.* **1964**, *86*, 3024.
[9] T. A. Coffey, G. D. Forster, G. Hogarth, *J. Chem. Soc. Dalton Trans.* **1995**, 2337.
[10] a) M. Minelli, R. L. Kuhlman, S. J. Shaffer, M. Y. Chiang, *Inorg. Chem.* **1992**, *31*, 3891; b) M. Minelli, M. R. Carson, D. W. Whisenhunt, J. L. Hubbard Jr, *Inorg. Chem.* **1990**, *29*, 442; c) M. Minelli, M. R. Carson, D. W. Whisenhunt, W. Imhof Jr, G. Huttner, *Inorg. Chem.* **1990**, *29*, 4801.
[11] a) E. A. Maatta, B. L. Haymore, R. A. D. Wentworth, *Inorg. Chem.* **1980**, *19*, 1055; b) L. O. Atovmyan, V. V. Tkachen, S. A. Shchepinov, *Sov. J. Coord. Chem. (Engl. Transl.)* **1978**, *4*, 460; c) K. L. Wall, K. Folting, J. C. Huffman, R. A. D. Wentworth, *Inorg. Chem.* **1983**, *22*, 1756.
[12] a) G. Bahr, B. Schleltzer, *Chem. Ber.* **1955**, *88*, 1771; b) G. Bahr, *Angew. Chem.* **1956**, *68*, 525; c) E. I. Stiefel, L. E. Bennett, Z. Dori, T. H. Crawford, C. Simo, H. B. Gray, *Inorg. Chem.* **1970**, *9*, 281; d) A. Davison, R. H. Holm, *Inorg. Synth.* **1967**, *10*, 8.
[13] a) L. G. Howell, I. Fridovich, *J. Biol. Chem.* **1968**, *243*, 5941–5947; b) D. L. Kessler, K. V. Rajagopalan, *J. Biol. Chem.* **1972**, *247*, 6566–6573; c) D. L. Kessler, K. V. Rajagopalan, *Biochim. Biophys. Acta* **1974**, *370*, 399–409; d) J. L. Johnson, K. V. Rajagopalan, *J. Clin. Invest.* **1978**, *58*, 543–550; e) S. P. Kramer, J. L. Johnson, A. A. Ribeiro, D. S. Mullington, K. V. Rajagopalan, *J. Biol. Chem.* **1987**, *262*, 16357; f) G. N. George, I. J. Pickering, C. Kisker, *Inorg. Chem.* **1999**, *38*, 2539–2540; g) C. Kisker, H. Schindelin, A. Pacheco, W. A. Wehbi, R. M. Garrett, K. V. Rajagopalan, J. H. Enemark, D. C. Rees, *Cell* **1997**, *91*, 973–983; h) H. K. Joshi, J. A. Cooney, F. E. Inscore, N. E. D. Gruhn, L. Lichtenberger, J. H. Enemark, *Proc. Natl. Acad. Sci. USA* **2003**, *100*, 3719–3724.
[14] A. Kay, P. C. H. Mitchell, *J. Chem. Soc. A* **1970**, 2421–2428.
[15] P. K. Chaudhury, K. Nagarajan, A. Kumar, R. Maiti, S. K. Das, S. Sarkar, *Indian J. Chem. Sect. A* **2003**, *42*, 2223.
[16] C. G. Young, *Molybdenum*, in *Comprehensive Coordination Chemistry II* (Eds.: J. A. McCleverty, T. J. Meyer, A. G. Wedd), Pergamon, Oxford, pp. 461.
[17] a) E. I. Stiefel, in *Molybdenum and Molybdenum-Containing Enzymes*, 1st ed. (Ed.: M. P. Coughlan), Pergamon Press, Oxford, **1980**, pp. 80–64; b) Book of Abstracts, *Second International Conference on the Chemistry and Uses of Molybdenum*, New Collage, Oxford, England, 30 Aug.–03 Sept., **1976**, pp. 265–269; c) K. Yamanouchi, J. H. Enmark, *Inorg. Chem.* **1978**, *17*, 2911–2917; d) J. K. Garner, N. Pariyadath, J. L. Corbin, E. I. Stiefel, *Inorg. Chem.* **1978**, *17*, 897–904.
[18] a) F. A. Cotton, *J. Chem. Educ.* **1983**, *60*, 713–720; b) F. A. Cotton, *Chem. Soc. Rev.* **1975**, *4*, 27; c) F. A. Cotton, *Acc. Chem. Res.* **1978**, *11*, 225; d) F. A. Cotton, S. M. Morehouse, *Inorg. Chem.* **1965**, *4*, 1377–1381; e) F. A. Cotton, R. A. Walton, *Multiple Bonds between Metal Atoms*, 2nd ed., Clarendon Press, Oxford, **1993**; f) F. A. Cotton, G. Wilkinson, C. A. Murillo, M. Bochmann, *Advanced Inorganic Chemistry*, 6th ed., John Wiley & Sons, **1999**.
[19] a) L. Gagliardi, B. O. Roos, *Nature* **2005**, *433*, 845–851; b) T. Nguyen, A. D. Sutton, M. Brynda, J. C. Fettinger, G. J. Long, P. P. Power, *Science* **2005**, *310*, 844–847.
[20] a) T. Yamaguchi, F. Yamazaki, T. Ito, *J. Am. Chem. Soc.* **2001**, *123*, 734–744; b) C. Mealli, F. Pichierri, L. Randaccio, E. Zangrando, M. Krumm, D. Holtenrich, B. Lippert, *Inorg. Chem.* **1995**, *34*, 3418–3424.
[21] a) M. H. Chisholm, J. C. Huffman, G. William, *J. Am. Chem. Soc.* **1987**, *109*, 2514–2515; b) B. E. Bursten, W. F. Schneider, *Inorg. Chem.* **1989**, *28*, 3293–3296; c) M. H. Chisholm, J. C. Huffman, R. J. Tatz, *J. Am. Chem. Soc.* **1984**, *106*, 5385–5386.
[22] a) F. A. Cotton, P. E. Fanwick, J. W. Fitch, H. D. Glicksman, R. A. Walton, *J. Am. Chem. Soc.* **1979**, *101*, 1752–1757; b) S. A. Best, T. J. Smith, R. A. Walton, *Inorg. Chem.* **1978**, *17*, 99–104.
[23] A. Altomare, M. C. Burla, M. Camalli, G. L. Cascarano, C. Giacovazzo, A. Guagliardi, A. G. G. Moliterni, G. Polidori, R. Spagna, *J. Appl. Crystallogr.* **1999**, *32*, 115–119.
[24] G. M. Sheldrick, *SHELX97: A Program for Crystal Structure Analysis* (release 97-2), University of Göttingen, Germany, **1997**.
[25] L. J. Farrugia, *J. Appl. Crystallogr.* **1997**, *30*, 565.
[26] *Gaussian 03*, Revision B.05, M. J. Frisch, G. W. Trucks, H. B. Schlegel, G. E. Scuseria, M. A. Robb, J. R. Cheeseman, J. A. Montgomery Jr, T. Vreven, K. N. Kudin, J. C. Burant, J. M. Millam, S. S. Iyengar, J. Tomasi, V. Barone, B. Mennucci, M. Cossi, G. Scalmani, N. Rega, G. A. Petersson, H. Nakatsuji, M. Hada, M. Ehara, K. Toyota, R. Fukuda, J. Hasegawa, M. Ishida, T. Nakajima, Y. Honda, O. Kitao, H. Nakai, M. Klene, X. Li, J. E. Knox, H. P. Hratchian, J. B. Cross, C. Adamo, J. Jaramillo, R. Gomperts, R. E. Stratmann, O. Yazyev, A. J. Austin, R. Cammi, C. Pomelli, J. W. Ochterski, P. Y. Ayala, K. Morokuma, G. A. Voth, P. Salvador, J. J. Dannenberg, V. G. Zakrzewski, S. Dapprich, A. D. Daniels, M. C. Strain, O. Farkas, D. K. Malick, A. D. Rabuck, K. Raghavachari, J. B. Foresman, J. V. Ortiz, Q. Cui, A. G. Baboul, S. Clifford, J. Cioslowski, B. B. Stefanov, G. Liu, A. Liashenko, P. Piskorz, I. Komaromi, R. L. Martin, D. J. Fox, T. Keith, M. A. Al-Laham, C. Y. Peng, A. Nanayakkara, M. Challacombe, P. M. W. Gill, B. Johnson, W. Chen, M. W. Wong, C. Gonzalez, J. A. Pople, Gaussian, Inc., Pittsburgh PA, **2003**.
[27] a) A. D. Becke, *J. Chem. Phys.* **1993**, *98*, 5648; b) C. Lee, W. Yang, R. G. Par, *Phys. Rev. B* **1988**, *37*, 785.
[28] G. A. Patersson, M. A. Al-Laham, *J. Chem. Phys.* **1991**, *94*, 6081.
[29] P. J. Hay, W. R. Wadt, *J. Chem. Phys.* **1985**, *82*, 299.
[30] a) P. J. Hey, W. R. Wadt, *J. Chem. Phys.* **1985**, *82*, 270–283; b) W. R. Wadt, P. J. Hey, *J. Chem. Phys.* **1985**, *82*, 284–298.
[31] a) P. E. Smith, R. M. Brunne, A. E. Mark, W. F. Gunsteren, *J. Phys. Chem.* **1993**, *97*, 2009–2014; b) G. Löffler, H. Schreiber, O. Steinhauser, *J. Mol. Biol.* **1997**, *270*, 520–534; c) F. Ogliaro, S. P. de Visser, S. Cohen, P. K. Sharma, S. Shaik, *J. Am. Chem. Soc.* **2002**, *124*, 2806–2814.

Received: June 17, 2007
Published Online: October 9, 2007

